INTERNATIONAL JOURNAL FOR NUMERICAL METHODS IN FLUIDS, VOL. 20, 1137–1151 (1995)

A COMPACT FOURTH-ORDER FINITE DIFFERENCE SCHEME FOR THE STEADY INCOMPRESSIBLE NAVIER–STOKES EQUATIONS

MING LI AND TAO TANG

Department of Mathematics and Statistics, Simon Fraser University, Burnaby, B. C., Canada V5A 1S6

AND

BENGT FORNBERG

Corporate Research, Exxon Research and Engineering Company, Annandale, NJ 08801, U.S.A.

SUMMARY

We note in this study that the Navier–Stokes equations, when expressed in streamfunction–vorticity form, can be approximated to fourth-order accuracy with stencils extending only over a 3×3 square of points. The key advantage of the new compact fourth-order scheme is that it allows direct iteration for low-to-medium Reynolds numbers. Numerical solutions are obtained for the model problem of the driven cavity and compared with solutions available in the literature. For $Re \leq 7500$ point-SOR iteration is used and the convergence is fast.

KEY WORDS: Navier–Stokes equations; streamfunction; vorticity; compact scheme; driven cavity problem

1. INTRODUCTION

The present paper is concerned with solving the steady two-dimensional Navier–Stokes (N–S) equations by finite differences. It is known that finite difference (FD) methods of obtaining approximate numerical solutions of the steady incompressible N–S equations can vary considerably in terms of accuracy and efficiency. In the area of FD methods it has been discovered that although central difference approximations are locally second-order-accurate, they often suffer from computational instability and the resulting solutions exhibit non-physical oscillations. The upwind difference approximations are computationally stable, although only first-order-accurate, and the resulting solutions exhibit the effects of artificial viscosity. The second-order upwind methods are no better than the first-order upwind difference ones for large values of *Re*. The higher-order FD methods of conventional type do not allow direct iterative techniques. An exception has been found in the high-order FD schemes of compact type, which are computationally efficient and stable and yield highly accurate numerical solutions.[1–3]

CCC 0271–2091/95/101137–15

Received 24 March 1994
Revised 23 August 1994

The approximation

$$\frac{1}{6h^2}\begin{bmatrix}1 & 4 & 1\\ 4 & -20 & 4\\ 1 & 4 & 1\end{bmatrix}\psi = -\frac{1}{12}\begin{bmatrix} & 1 & \\ 1 & 8 & 1\\ & 1 & \end{bmatrix}\zeta \tag{1}$$

to the equation

$$\frac{\partial^2\psi}{\partial x^2}+\frac{\partial^2\psi}{\partial y^2} = -\zeta \tag{2}$$

is fourth-order accurate when applied to any solutions to equation (2). Gupta *et al.*,[4] Dennis and Hudson[2] and Gupta[3] note that this technique can be generalized to also provide a fourth-order-accurate nine-point scheme for solutions to the convection–diffusion equation

$$\frac{\partial^2\zeta}{\partial x^2}+\frac{\partial^2\zeta}{\partial y^2}-Re\left(p(x,\,y)\frac{\partial\zeta}{\partial x}+q(x,\,y)\frac{\partial\zeta}{\partial y}\right)=f(x,\,y). \tag{3}$$

With the choices $p(x, y) = \psi_y$, $q(x, y) = -\psi_x$ and $f(x, y) = 0$ the pair of equations (2), (3) forms the steady 2D N–S equations. However, in this case a problem arises in that the approximations needed to obtain the velocities $p(x, y)$ and $q(x, y)$ to fourth-order accuracy will extend outside the (3×3)-point domain.[2,3] In the present work we derive a compact fourth-order FD scheme for the time-independent N–S equations with the novelty of 'genuine compactness', i.e. the compact scheme is strictly within the nine-point stencil. It is shown that the new scheme yields highly accurate numerical solutions while still allowing SOR-type iterations for low-to-medium Reynolds numbers.

The organization of the paper is as follows. In the next section we introduce the compact fourth-order FD scheme for the N–S equations. In Section 3 we test the new fourth-order scheme for the N–S equations which possess an exact solution. The model problem of the lid-driven cavity is described in Section 4 with detailed comparisons of our solutions with the existing solutions in the literature. In Section 5 we discuss possible extensions of the present method.

2. NUMERICAL METHODS

The N–S equations representing the two-dimensional steady flow of an incompressible viscous fluid are given in streamfunction–vorticity form as

$$\frac{\partial^2\psi}{\partial x^2}+\frac{\partial^2\psi}{\partial y^2} = -\zeta, \tag{4}$$

$$\frac{\partial^2\zeta}{\partial x^2}+\frac{\partial^2\zeta}{\partial y^2} = Re\left(\frac{\partial\psi}{\partial y}\frac{\partial\zeta}{\partial x}-\frac{\partial\psi}{\partial x}\frac{\partial\zeta}{\partial y}\right). \tag{5}$$

Here ψ is the streamfunction, ζ is the vorticity and Re is the non-dimensional Reynolds number. Assuming a uniform grid in both x- and y-directions, we number the grid points (x, y), $(x+h, y)$, $(x, y+h)$, $(x-h, y)$, $(x, y-h)$, $(x+h, y+h)$, $(x-h, y+h)$, $(x-h, y-h)$ and $(x+h, y-h)$ as 0, 1, 2, 3, 4, 5, 6, 7 and 8 respectively (see Figure 1), where h is the grid size. In writing the FD approximations, a single subscript j denotes the corresponding function value at the grid point numbered j.

By (1), a compact fourth-order scheme for (4) follows immediately:

$$4(\psi_1+\psi_2+\psi_3+\psi_4)+\psi_5+\psi_6+\psi_7+\psi_8-20\psi_0 = -\frac{h^2}{2}(\zeta_1+\zeta_2+\zeta_3+\zeta_4+8\zeta_0). \tag{6}$$

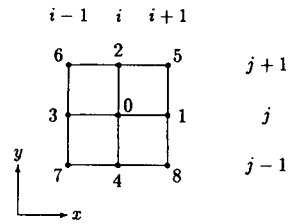

Figure 1. Computational stencil

Next, letting $g(x, y) = \psi_y\zeta_x - \psi s\zeta_y$, we can rewrite (5) as $\zeta_{xx} + \zeta_{yy} = Re\, g(x, y)$. Now, using (16) in the Appendix yields

$$8(\zeta_1 + \zeta_2 + \zeta_3 + \zeta_4) + 2(\zeta_5 + \zeta_6 + \zeta_7 + \zeta_8) - 40\zeta_0 = 12h^2\, Re\, g + h^4\, Re(g_{xx} + g_{yy}) + O(h^6).$$

Note that g consists of first partial derivatives of ψ and ζ. Then $g_{xx} + g_{yy}$ involves the third derivatives of ψ and ζ and this in turn will lead to the use of extra points outside the (3×3)-point domain and ruin the compactness. To avoid this, we replace the directional derivatives ψ_{xxx}, ψ_{yyy}, ζ_{xxx} and ζ_{yyy} be appropriate mixed derivatives which can be approximated up to $O(h^2)$ using the nine points. This strategy successfully gives a resulting scheme of fourth order at the cost of tedious but trivial manipulations. We defer the derivation to the Appendix and simply give the result here:

$$\begin{aligned}
&8(\zeta_1 + \zeta_2 + \zeta_3 + \zeta_4) + 2(\zeta_5 + \zeta_6 + \zeta_7 + \zeta_8) - 40\zeta_0 \\
&\quad = Re(\psi_{24}\zeta_{13} - \psi_{13}\zeta_{24} + \psi_1\zeta_{85} + \psi_2\zeta_{56} + \psi_3\zeta_{67} + \psi_4\zeta_{78} + \psi_5\zeta_{12} + \psi_6\zeta_{23} + \psi_7\zeta_{34} + \psi_8\zeta_{41}) \\
&\qquad + \frac{Re^2}{4}\left[\psi_{13}\zeta_{13}\psi_{204} + \psi_{24}\zeta_{24}\psi_{103} + \tfrac{1}{2}\psi_{13}\psi_{24}(\zeta_{56} + \zeta_{78})\right. \\
&\qquad \left. - \tfrac{1}{4}(\psi_{13}\zeta_{24} + \psi_{24}\zeta_{13})(\psi_{56} + \psi_{78}) - \psi_{13}^2\zeta_{204} - \psi_{24}^2\zeta_{103}\right],
\end{aligned} \tag{7}$$

where $f_{ij} := f_i - f_j$ and $f_{ikj} := f_i - 2f_k + f_j$. The fourth-order compact scheme for the N–S equations (4) and (5) is given by (6) and (7).

The new fourth-order compact scheme (6) and (7) is to be solved by pointwise iteration methods as described in Reference 5 or by Newton's method with direct solvers at each stage as described in Reference 6.

3. NAVIER–STOKES EQUATIONS WITH EXACT SOLUTION

In this section we obtain numerical solutions of (4) and (5) using the new fourth-order compact scheme (6), (7). The test problem used in this section is chosen such that the analytical solution is available, so a rigorous comparison can be made. Following Reference 7, we give the test problem which has exact solutions for the N–S equations (4) and (5) in Ω:

$$\psi = \frac{y - x}{Re} - e^{x+y}, \qquad \zeta = 2e^{x+y}, \qquad \Omega = (0, 1) \times (0, 1)$$

We notice that the above solution is smooth in $\bar{\Omega} := [0, 1] \times [0, 1]$.

We consider the test problem with Dirichlet boundary conditions, i.e. boundary values of ψ and ζ are given. Various Reynolds numbers ranging from $Re = 5$ to 1000 were tested, but since the results appear to be Re-independent, only those for $Re = 1000$ are shown. For the sake of comparison the results using a second-order central difference scheme are also presented. The RMS errors in Ω for the streamfunction and vorticity are given in Table I. It is observed that the results for the h^2 scheme, the

Table I. RMS errors in Ω for the streamfunction and vorticity at $Re = 1000$

	ψ-error, ζ-error	ψ-error, ζ-error	ψ-error, ζ-error	ψ-error, ζ-error
h^2 scheme	1·41(−4)*, 2·71(−4)	3·35(−5), 6·63(−5)	8·17(−6), 1·63(−5)	2·02(−6), 4·01(−6)
h^4 scheme	4·72(−8), 9·45(−8)	2·80(−9), 5·59(−9)	1·70(−10), 3·40(−10)	1·05(−11), 2·10(−11)
Grid	11 × 11	21 × 21	41 × 41	81 × 81

* $1{\cdot}41(-4) = 1{\cdot}41 \times 10^{-4}$, etc.

central difference scheme, are in good agreement with those obtained by Bramley and Sloan.[8] It is also seen that the convergence orders for the h^2 scheme and the h^4 scheme, (6) and (7), are two and four respectively. This confirms that the compact scheme (6), (7) is of fourth-order accuracy when the solutions of (4) and (5) are smooth.

This test problem is solved by Newton's method. The Newton iteration process is similar to that described in Reference 6. In all the calculations, less than four iterations are required in order to obtain convergent results.

4. DRIVEN CAVITY PROBLEM

As a model problem we consider the steady flow of an incompressible viscous fluid in a square cavity ($0 \leq x \leq 1, 0 \leq y \leq 1$). The flow is induced by the sliding motion of the top wall ($y = 1$) from left to right; see Figure 2. The boundary conditions are those of no slip: on the stationary walls $u = \partial\psi/\partial y = 0$ and $v = -\partial\psi/\partial x = 0$; on the sliding wall $u = 1$ and $v = 0$. This problem has served over and over again as a model problem for testing and evaluating numerical techniques, in spite of the singularities at two of its corners. Highly accurate benchmark solutions of this problem are available in the literature (see e.g. References 9 and 10).

4.1. Numerical boundary conditions

The implementation of numerical boundary conditions has received considerable attention in the past. Basically there is at least two topics worth discussing in detail: the vorticity condition on the boundary and the influence of boundary accuracy (less than the interior) versus global accuracy. For the first topic, in spite of the fact that the numerical boundary condition involving the vorticity on the boundary has been proved practically successful, it is argued that specifying the vorticity on the boundary does not coincide with the reality either physically or mathematically (see e.g. Reference 11).

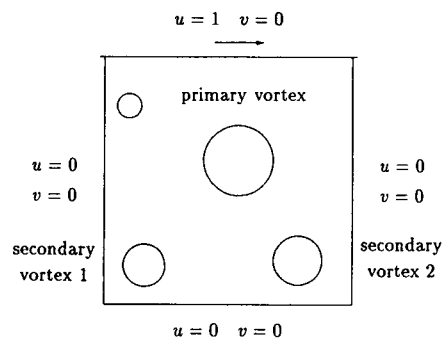

Figure 2. Driven cavity

From this point of view it is proposed to use two boundary conditions on ψ and none on ζ (see e.g. References 11 and 12). As to accuracy, it is not quite clear whether less accuracy on the boundary would essentially depreciate the global accuracy, since a rigorous error analysis is by no means easy for the resulting non-linear scheme. Nevertheless, a recent work by Hou and Wetton[13] proved that global second-order accuracy can be obtained via a second-order-accurate difference scheme in the interior and a first-order-accurate method on the boundary.

In this work our numerical boundary condition is based on the theory in Reference 11. It uses two conditions on ψ: on the stationary walls $\psi_0 = 0$ and $\psi_1 = \psi_2/2 - \psi_3/9$; on the moving wall $y = 1$, $\psi_0 = 0$ and $\psi_1 = \psi_2/2 - \psi_3/9 + h/3$. Here the subscript 0 denotes a value at a boundary grid point and the subscript j ($j = 1, 2, 3$) denotes values at the jth internal grid point along the inward normal at 0. The boundary conditions for ψ are based on the fact that

$$\frac{1}{3h}\psi_3 - \frac{3}{2h}\psi_2 + \frac{3}{h}\psi_1 - \frac{11}{6h}\psi_0$$

is a third-order-accurate approximation of $\partial\psi/\partial n$. The vorticity ζ_1 is determined by the standard five-point FD method for (4). The compact scheme (6), (7) is to be implemented in the region $[2h, 1-2h] \times [2h, 1-2h]$. It can be verified that this treatment of the numerical boundary condition has second-order accuracy for ζ_1 in the sense of truncation errors. Moreover, it can be seen that the values of ζ_0 are not used in the calculations. For detail of this method see Reference 12.

4.2. *Comparisons with existing solutions*

We now present numerical solutions for the driven cavity problem for $Re \leq 7500$. To illustrate the advantages of the compact fourth-order scheme, we shall concentrate on the following two points.

1. *Efficiency.* We show that the non-linear systems can be solved by using the point-SOR iteration method.
2. *Accuracy.* We use mesh sizes which are greater than those used in References 9 and 10 to obtain qualitatively and quantitatively agreeable results for reasonably large values of the Reynolds number.

The unit square is covered by a grid of uniform mesh size h ($h = 1/N$). Numerical solutions are obtained using an inner–outer iteration procedure as described in Reference 5. At each outer iteration the non-linear systems from the discrete streamfunction and vorticity equations are solved iteratively. We solve these non-linear systems using point-SOR iteration with the relaxation parameters $\alpha \geq 1$ for the streamfunction and $\beta \geq 1$ for the vorticity. These parameters are usually taken as $\alpha = 1{\cdot}5$ and $\beta = 1{\cdot}2$ for the coarse mesh (41×41 grid). For the fine mesh (129×129 grid) we use $(\alpha, \beta) = (1{\cdot}2, 1{\cdot}1)$ for $Re \leq 3200$ and $(\alpha, \beta) = (1{\cdot}1, 1{\cdot}0)$ for $Re > 3200$. We also use two inner iterations in all the calculations. The smoothing (or damping) parameter δ is used to obtain the numerical boundary values.

Let

$$E(m) = \sum_{i,j} |\zeta_{ij}^{(m)} - \zeta_{ij}^{(m-1)}| + \sum_{i,j} |\psi_{ij}^{(m)} - \psi_{ij}^{(m-1)}| \tag{8}$$

denote the iteration error at the mth itertaion, where $\{\zeta_{ij}^{(m)}\}$ and $\{\psi_{ij}^{(m)}\}$ refer to the values of $\{\zeta_{ij}\}$ and $\{\psi_{ij}\}$ after the mth iteration. To show the rate of convergence, we plot the convergence history for $Re = 100$, 400, 1000 and 2000 using a 41×41 grid in Figure 3. The iterations were started with zero initial data and were terminated when $E(m) < 10^{-4}$. The relaxation parameters used are $(\alpha, \beta, \delta) = (1{\cdot}5, 1{\cdot}2, 0{\cdot}9)$ for $Re \leq 1000$ and $(\alpha, \beta, \delta) = (1{\cdot}2, 1{\cdot}1, 0{\cdot}5)$ for $Re = 2000$. Moreover, in Table II we give the number of outer iterations needed to converge to the required tolerance. Table II

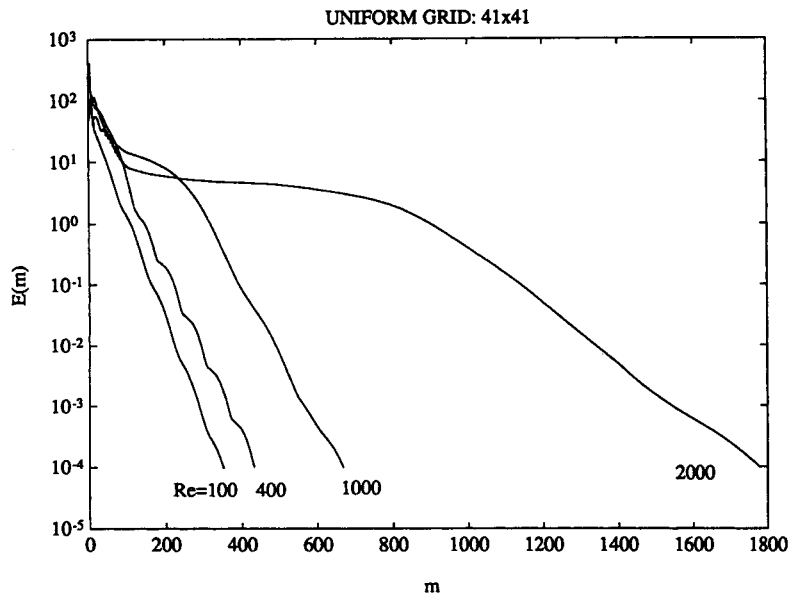

Figure 3. Convergence history for $Re = 100$, 400, 1000 and 2000

also includes the corresponding numbers provided in Reference 3. It is seen that the present procedure is faster than that used in Reference 3.

For the fine grid (129 × 129) the solution procedure is as follows. First we set $Re = 200$ and use zero initial values. When $E(m) < \gamma = 0{\cdot}05$, we increase the value of the Reynolds number by letting $Re = Re + \Delta R$ with $\Delta R = 200$. If the iteration error $E(m)$ for this Re is less than γ, we increase the value of Re by adding another ΔR. Repeat this procedure until $Re = 1000$. Then more iterations are used until $E(m) < 5 \times 10^{-4}$; see Figure 4(a). Thus we obtain the convergent solutions for $Re = 1000$. Next we set $Re = 1200$ and use the solutions for $Re = 1000$ as starting values. If $E(m) < \gamma = 0{\cdot}05$, then the value of Re is updated by adding a ΔR which again equals 200. Repeat this procedure until $Re = 3200$. Then more iterations are used until $E(m) < 5 \times 10^{-4}$; see Figure 4(a). Similarly we use the convergent solutions for $Re = 3200$ and 5000 as initial values for $Re = 5000$ and 7500 respectively, but in these two cases we use $\Delta R = 50$ and $\gamma = 0{\cdot}01$; see Figure 4(b). The relaxation parameters are $(\alpha, \beta, \delta) = (1{\cdot}2, 1{\cdot}1, 0{\cdot}9)$ for $Re \leq 3200$ and $(\alpha, \beta, \delta) = (1{\cdot}1, 1{\cdot}0, 0{\cdot}5)$ for $Re > 3200$. It can be seen from Figure 4 that about 4000 iterations are sufficient to obtain convergent solutions for all the Reynolds numbers considered.

Table II. Number of outer iterations needed to converge to 10^{-4}. The present calculation uses two inner iterations. Ten inner iterations are used by Gupta[3]

Re	Present	Gupta
100	352	353
400	433	509
1000	668	1040
2000	1779	4266

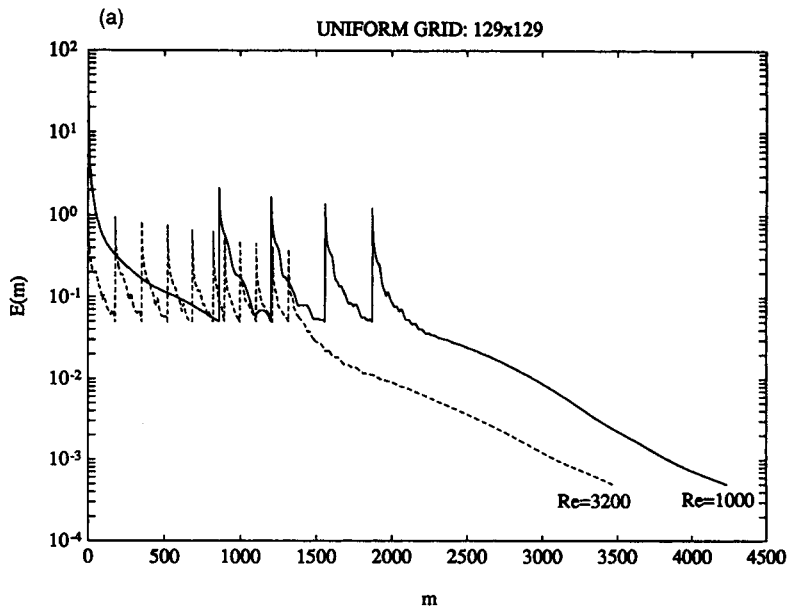

Figure 4(a). Convergence history for Re = 1000 and 3200

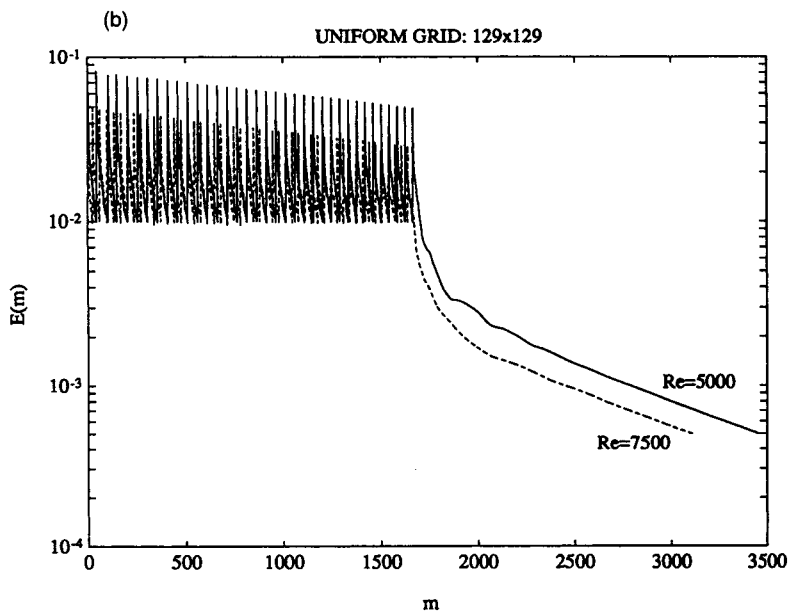

Figure 4(b). Convergence history for Re = 5000 and 7500

Figures 5 and 6 show the streamfunction and vorticity contours for $Re = 1$, 100, 400 and 1000 using a 41×41 grid. They can be compared with the results of Gupta,[3] Ghia *et al.*[9] and Schreiber and Keller[10] and are graphically indistinguishable. Figures 7 and 8 show the streamfunction and vorticity contours for $Re = 1000$, 3200, 5000 and 7500 using a 129×129 grid. Again they compare well with the well-known results obtained by Ghia *et al.*[9] In Table III we summarize the data concerning the locations and strengths of the primary vortex for $Re = 1000$, 3200, 5000 and 7500, which are found to be in very good agreement with the higher-order results in Reference 14 and the finer mesh results in Reference 9.

5. EXTENSIONS

5.1. *Extension to rectangular grids*

The schemes introduced in Section 2 can be readily extended to rectangular grids, i.e. the mesh sizes Δx in the x-direction and Δy in the y-direction are different. The derivation is in the same spirit as the Appendix. We use Taylor expansion in the x- and y-directions separately when discretizing the differential equations. In invoking equations (4) and (5) to eliminate third-order directional derivatives (as in the Appendix, equations (17) and (19)), we use

$$-\psi_{xxx} = \psi_{yyx} + \zeta_x, \qquad \zeta_{xxx} = Re\, g_x - \zeta_{xyy}, \tag{9}$$

$$\psi_{yyy} = -\zeta_y - \psi_{xxy}, \qquad -\zeta_{yyy} = -Re\, g_y + \zeta_{xxy}. \tag{10}$$

Finally we can obtain the fourth-order compact scheme with anisotropic mesh size for (4) and (5):

$$\begin{aligned}(10\lambda - 2\gamma)(\psi_1 + \psi_3) + (10\gamma - 2\lambda)(\psi_2 + \psi_4) + (\lambda + \gamma)(\psi_5 + \psi_6 + \psi_7 + \psi_8 - 20\psi_0)\\ = -\Delta x \Delta y(\zeta_1 + \zeta_2 + \zeta_3 + \zeta_4 + 8\zeta_0),\end{aligned}$$

Table III. Comparison of the results on features of the primary vortex for high Reynolds numbers

Re	Source	ψ-value	ζ- value	Location
1000	Present (129×129)	0·118448	2·05876	0·5313, 0·5625
	Nishida and Satofuka[14] (129×129)	0·119004	2·06855	0·5313, 0·5625
	Ghia *et al.*[9] (129×129)	0·117929	2·04968	0·5313, 0·5625
3200	Present (129×129)	0·120529	1·94286	0·5156, 0·5391
	Nishida and Satofuka[14] (129×129)	0·121154	1·95078	0·5156, 0·5391
	Ghia *et al.*[9] (129×129)	0·120377	1·98860	0·5165, 0·5469
5000	Present (129×129)	0·120359	1·92430	0·5156, 0·5391
	Ghia *et al.*[9] (257×257)	0·118966	1·86016	0·5117, 0·5352
7500	Present (129×129)	0·119379	1·91950	0·5156, 0·5391
	Ghia *et al.*[9] (257×257)	0·119976	1·87987	0·5117, 0·5322

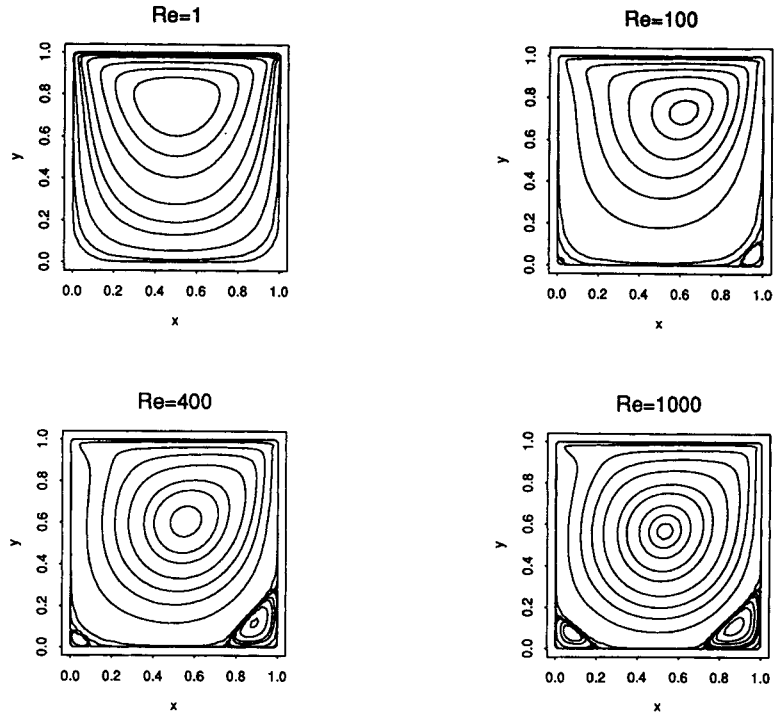

Figure 5. Streamlines for $Re = 1$, 100, 400 and 1000 using a 41×41 uniform grid

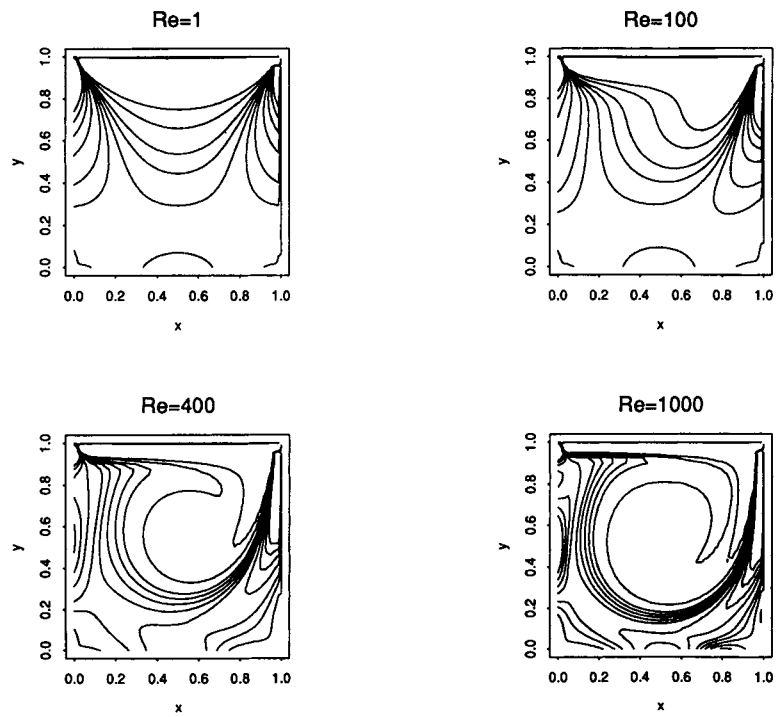

Figure 6. Vorticity contours for $Re = 1$, 100, 400 and 1000 using a 41×41 uniform grid

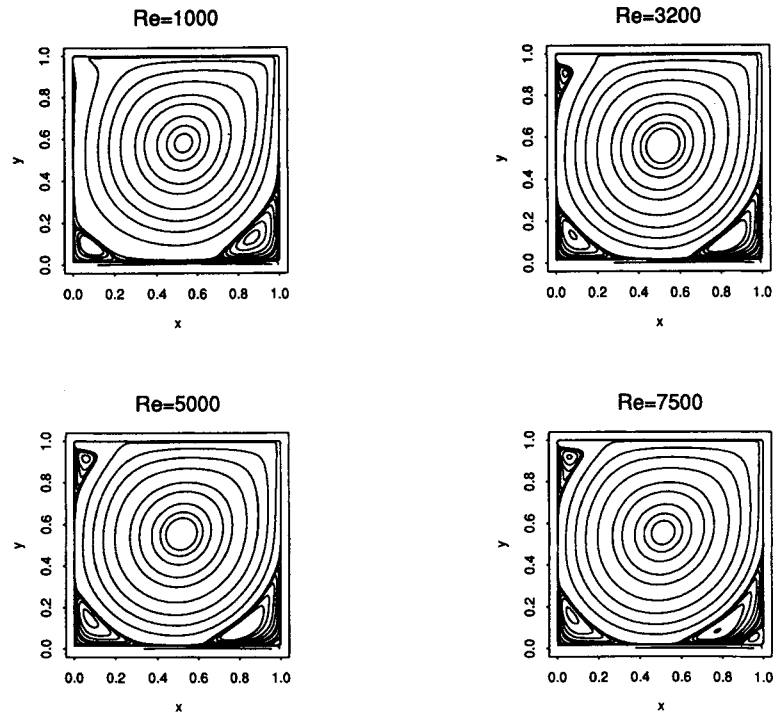

Figure 7. Streamlines for $Re = 1000$, 3200, 5000 and 7500 using a 129×129 uniform grid

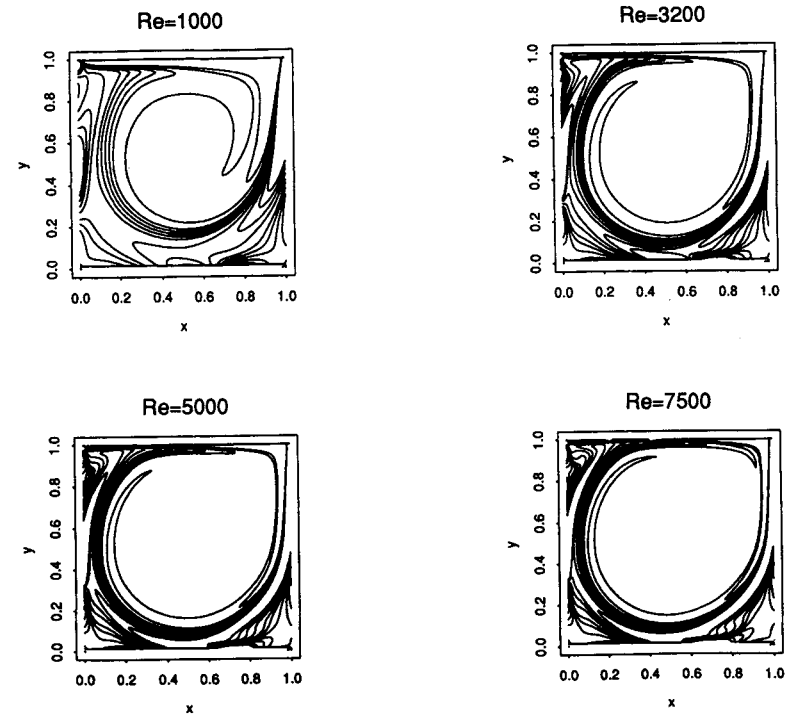

Figure 8. Vorticity contours for $Re = 1000$, 3200, 5000 and 7500 using a 129×129 uniform grid

$$
\begin{aligned}
&(10\lambda - 2\gamma)(\zeta_1 + \zeta_3) + (10\gamma - 2\lambda)(\zeta_2 + \zeta_4) + (\lambda + \gamma)(\zeta_5 + \zeta_6 + \zeta_7 + \zeta_8 - 20\zeta_0) \\
&\quad = \frac{Re}{2}(4 - \lambda^2 - \gamma^2)(\psi_{24}\zeta_{13} - \psi_{13}\zeta_{24}) + \frac{Re}{4}(\Delta y^2 - \Delta x^2)\zeta_{13}\zeta_{24} \\
&\qquad + \frac{Re}{4}[\psi_1(\zeta_{67} + 3\zeta_{85}) + \psi_2(\zeta_{78} + 3\zeta_{56}) + \psi_3(\zeta_{85} + 3\zeta_{67}) + \psi_4(\zeta_{56} + 3\zeta_{78}) \\
&\qquad + \psi_5(\zeta_{34} + 3\zeta_{12}) + \psi_6(\zeta_{41} + 3\zeta_{23}) + \psi_7(\zeta_{12} + 3\zeta_{34}) + \psi_8(\zeta_{23} + 3\zeta_{41})] \\
&\qquad + \frac{\lambda^2 Re}{4}[\zeta_{13}(\psi_{57} + \psi_{68}) - \psi_{13}(\zeta_{57} + \zeta_{68})] + \frac{\gamma^2 Re}{4}[\psi_{24}(\zeta_{56} - \zeta_{78}) - \zeta_{24}(\psi_{56} - \psi_{78})] \\
&\qquad + \frac{Re^2}{4}\Big(\lambda\psi_{13}(\zeta_{13}\psi_{204} - \psi_{13}\zeta_{204}) + \gamma\psi_{24}(\zeta_{24}\psi_{103} = \psi_{24}\zeta_{103}) \\
&\qquad + \frac{\lambda + \gamma}{4}\psi_{13}\psi_{24}(\zeta_{56} + \zeta_{78}) - \tfrac{1}{4}(\gamma\psi_{24}\zeta_{13} + \lambda\psi_{13}\zeta_{24})(\psi_{56} + \psi_{78})\Big),
\end{aligned}
$$

where $\lambda = \Delta y/\Delta x$, $\gamma = \Delta x/\Delta y$ and again $f_{ij} := f_i - f_j$, $f_{ikj} := f_i - 2f_k + f_j$. It is easy to verify that when $\Delta x = \Delta y$, the above scheme is in coincidence with the one given in Section 2. In order for the above scheme to allow SOR-type iteration, the mesh ratio γ is required to satisfy $\gamma \in (1/\sqrt{5}, \sqrt{5})$.

5.2. Extension to more general domains

If a domain can be transformed into a rectangular one by *conformal* mappings, then the present compact fourth-order methods can be extended to solve the transformed equations in the rectangular domain. By using a conformal mapping $x = x(\sigma, \eta)$ and $y = y(\sigma, \eta)$, the resulting N–S equations can be written as

$$\psi_{\sigma\sigma} + \psi_{\eta\eta} = -\beta(\sigma, \eta)\zeta, \tag{11}$$

$$\zeta_{\sigma\sigma} + \zeta_{\eta\eta} = Re\Big(\psi_\eta\zeta_\sigma - \psi_\sigma\zeta_\eta\Big), \tag{12}$$

where $\beta(\sigma, \eta)$ is a known function. A fourth-order compact scheme for (11) and (12) can be constructed in similar way to the Appendix. The only extra steps are to add the term $\zeta(\beta_\sigma\zeta_\eta - \beta_\eta\zeta_\sigma)$ to the right-hand sides of (17) and (19). Since β_σ and β_η are known functions, the extra term can be readily approximated up to $O(h^2)$ within the nine-point stencil.

6. REMARKS AND CONCLUSIONS

6.1. Newton's method

Over recent years there has been great interest in using Newton's method with direct solvers at each stage to solve the discretized N–S equations. This technique is useful in obtaining accurate steady solutions not only in high-Reynolds-number cases but also in time-unstable situations such as steady incompressible flow past 'simple' blunt bodies (e.g. a cylinder, a sphere, a flat plate perpendicular to a freestream, arrays of such bodies, etc). In spite of the fact that experiments become time-dependent at relatively low Reynolds numbers (owing to instabilities), there are many reasons for studying steady (unstable) flow fields at high Reynolds numbers.[6,15,16] To obtain the steady (unstable) flow fields at high Reynolds numbers, it is impossible to employ any standard pointwise iterative methods, which tend to pick up instabilities reminiscent of temporal ones. The quadratic convergence of Newton's method precludes this from happening. The cost of solving banded systems with partially pivoted

Gaussian elimination is proportional to the number of iterations and to the square of the bandwidth. If we consider Newton's method implemented on an $N \times N$ grid, then with the usual row or column ordering the bandwidth for the previous compact fourth-order schemes[2,3] is $6N$. Therefore the cost of solving banded systems is $O(72N^4)$. On the other hand, the bandwidth for the present compact scheme is $4N$ and hence the cost of solving banded systems is $O(32N^4)$.

6.2. *Non-compact fourth-order schemes*

Hou and Wetton[17] employed fourth-order streamfunction methods for the *time-dependent*, incompressible N–S equations. Wide schemes which are built using standard fourth-order difference operators are employed instead of compact ones and the boundary terms are handled by extrapolating the streamfunction values. Evidence is given that this approach is preferable to using compact differencing for high-Reynolds-number flows. This property of compact schemes has been well documented in Reference 18. Indeed, we found that for the driven cavity problem the convergence becomes slow and SOR pointwise iteration does not work when $Re \geq 9000$. One of the reasons for this is that the truncation errors for all the compact schemes are of order $O(h^4Re^2)$, while the truncation errors for conventional fourth-order schemes are of order $O(h^4Re)$.

6.3. *Conclusions*

In this work we have developed a new compact fourth-order scheme for the time-independent Navier–Stokes equations with the novelty of 'genuine compactness'. In deriving compact fourth-order schemes, the main difference between our method and previous ones is the following. To obtain a compact fourth-order scheme for (5), previous researchers employ Taylor expansion for (5) but do not use (4) which gives the relation between ψ and ζ. However, our procedure also employs equation (4), so that the compact scheme for (5) is strictly within the nine-point stencil (see equations (17) and (19) in the Appendix). The key point with the present scheme is that it allows direct iteration for low-to-medium Re.

ACKNOWLEDGEMENTS

This research was supported by the Natural Sciences and Engineering Research Council of Canada under Grant OGP0105545. We are grateful to the referees for helpful suggestions that have improved the presentation of this paper.

APPENDIX: FOURTH-ORDER SCHEME FOR VORTICITY EQUATION

For completeness we first reiterate the derivation of the fourth-order compact scheme for

$$u_{xx} + u_{yy} = f(x, y). \tag{13}$$

Following the notation in Reference 19 and using Taylor expansion, we have (at point 0)

$$\delta_x^2 u = \frac{\partial^2 u}{\partial x^2} + \frac{h^2}{12}\frac{\partial^4 u}{\partial x^4} + O(h^4) = \left(1 + \frac{h^2}{12}\delta_x^2\right)\frac{\partial^2 u}{\partial x^2} + O(h^4),$$

where $\delta_x^2 := (u_1 - 2u_0 + u_3)/h$ (see Figure 1) and we have used the fact

$$\frac{\partial^2 u}{\partial x^2} = \delta_x^2 u + O(h^2). \tag{14}$$

Therefore, symbolically,

$$\frac{\partial^2}{\partial x^2} = \left(1 + \frac{h^2}{12}\delta_x^2\right)^{-1} \delta_x^2 + O(h^4).$$

Using the above formula and its counterpart in the y-direction, we can approximate (13) by

$$\left(1 + \frac{h^2}{12}\delta_x^2\right)^{-1} \delta_x^2 u + \left(1 + \frac{h^2}{12}\delta_y^2\right)^{-1} \delta_y^2 u = f + O(h^4),$$

which gives

$$\begin{aligned}\left(1 + \frac{h^2}{12}\delta_y^2\right)\delta_x^2 u + \left(1 + \frac{h^2}{12}\delta_x^2\right)\delta_y^2 u &= \left(1 + \frac{h^2}{12}\delta_x^2\right)\left(1 + \frac{h^2}{12}\delta_y^2\right) f + O(h^4) \\ &= \left(1 + \frac{h^2}{12}(\delta_x^2 + \delta_y^2)\right) f + O(h^4).\end{aligned} \tag{15}$$

Simplifying this expression, we can readily obtain (6). For (7) we first denote

$$g(x, y) = \psi_y \zeta_x - \psi_x \zeta_y.$$

Applying (14) and (15) to $\zeta_{xx} + \zeta_{yy} = Re\, g(x, y)$ yields

$$\begin{aligned}8(\zeta_1 + \zeta_2 + \zeta_3 + \zeta_4) + 2(\zeta_5 + \zeta_6 + \zeta_7 + \zeta_8) - 40\zeta_0 &= 12h^2\, Re\, g + h^4\, Re\,(g_{xx} + g_{yy}) + O(h^6) \\ &=: I_1 + I_2 + O(h^6).\end{aligned} \tag{16}$$

Straightforward calculations give us

$$\begin{aligned}g_x &= \psi_{yx}\zeta_x + \psi_y\zeta_{xx} - \psi_{xx}\zeta_y - \psi_x\zeta_{yx}, \\ g_y &= \psi_{yy}\zeta_x + \psi_y\zeta_{xy} - \psi_{xy}\zeta_y - \psi_x\zeta_{yy}, \\ g_{xx} &= \psi_{yxx}\zeta_x + 2\psi_{yx}\zeta_{xx} + \psi_y\zeta_{xxx} - \psi_{xxx}\zeta_y - 2\psi_{xx}\zeta_{yx} - \psi_x\zeta_{yxx}, \\ g_{yy} &= \psi_{yyy}\zeta_x + 2\psi_{yy}\zeta_{xy} + \psi_y\zeta_{xyy} - \psi_{xyy}\zeta_y - 2\psi_{xy}\zeta_{yy} - \psi_x\zeta_{yyy}.\end{aligned}$$

Using (4) and $\zeta_{xx} + \zeta_{yy} = Re\, g(x, y)$, we have

$$\begin{aligned}g_{xx} + g_{yy} &= \zeta_x(\psi_{xx} + \psi_{yy})_y + \psi_y(\zeta_{xx} + \zeta_{yy})_x - \zeta_y(\psi_{xx} + \psi_{yy})_x \\ &\quad - \psi_x(\zeta_{xx} + \zeta_{yy})_y + 2\psi_{xy}(\zeta_{xx} - \zeta_{yy}) + 2\zeta_{yx}(\psi_{yy} - \psi_{xx}) \\ &= Re\, \psi_y g_x - Re\, \psi_x g_y + 2\psi_{xy}(\zeta_{xx} - \zeta_{yy}) + 2\zeta_{xy}(\psi_{yy} - \psi_{xx}).\end{aligned} \tag{17}$$

This result implies that $g_{xx} + g_{yy}$ is a combination of first and second derivatives of ψ and ζ, which can be approximated to a truncation error of order $O(h^2)$ by the 3×3 grid points. That is, I_2 in (16) can be approximated by ψ_j, ζ_j, $0 \le j \le 8$, giving a truncation error of order $O(h^6)$. We now consider the term I_1. First notice that

$$\begin{aligned}\psi_{13} &:= \psi_1 - \psi_3 = 2h\psi_x + \frac{h^3}{3}\psi_{xxx} + O(h^5), \\ \psi_{24} &:= \psi_2 - \psi_4 = 2h\psi_y + \frac{h^3}{3}\psi_{yyy} + O(h^5).\end{aligned}$$

The above results, together with similar ones for ζ, yield

$$\psi_{24}\zeta_{13} - \psi_{13}\zeta_{24} = 4h^2 g + \frac{2h^4}{3}(\psi_y\zeta_{xxx} + \zeta_x\psi_{yyy} - \psi_x\zeta_{yyy} - \zeta_y\psi_{xxx}) + O(h^6). \tag{18}$$

This result implies that approximations for $h^2 g$ (or, equivalently, for I_1) may involve the use of ψ_{xxx}, ψ_{yyy}, ζ_{xxx}, ζ_{yyy}. However, in order to approximate these third derivatives to $O(h^2)$, extra points outside the (3×3)-point domain are required. To avoid this, we observe that

$$\begin{aligned}\psi_y\zeta_{xxx} + \zeta_x\psi_{yyy} - \psi_x\zeta_{yyy} - \zeta_y\psi_{xxx} &= \psi_y(\zeta_{xx} + \zeta_{yy})_x - \psi_y\zeta_{yyx} + \zeta(\psi_{xx} + \psi_{yy})_y - \zeta_x\psi_{xxy} \\ &\quad - \psi_x(\zeta_{xx} + \zeta_{yy})_y + \psi_x\zeta_{xxy} - \zeta(\psi_{xx} + \psi_{yy})_x + \zeta_y\psi_{yyx} \\ &= Re\,\psi_y g_x - Re\,\psi_x g_y - \psi_y\zeta_{yyx} - \zeta_x\psi_{xxy} + \psi_x\zeta_{xxy} + \zeta_y\psi_{yyx}. \end{aligned} \tag{19}$$

Combining (18) and (19) gives

$$12h^2 g = 3\psi_{24}\zeta_{13} - 3\psi_{13}\zeta_{24} - 2h^4(Re\,\psi_y g_x - Re\,\psi_x g_y - \psi_y\zeta_{yyx} - \zeta_x\psi_{xxy} + \psi_x\zeta_{xxy} + \zeta_y\psi_{yyx}) + O(h^6).$$

The above result, together with (17), yields

$$12h^2 g + h^4(g_{xx} + g_{yy}) = 3(\psi_{24}\zeta_{13} - \psi_{13}\zeta_{24}) + h^4(T_1 + T_2 + T_3) + O(h^6), \tag{20}$$

where

$$\begin{aligned} T_1 &= Re\,(\psi_x g_y - \psi_y g_x) \\ &= Re\,(\psi_x\zeta_x\psi_{yy} + \psi_y\zeta_y\psi_{xx} + 2\psi_x\psi_y\zeta_{xy} - \psi_x\zeta_y\psi_{xy} - \psi_y\zeta_x\psi_{xy} - \psi_x^2\zeta_{yy} - \psi_y^2\zeta_{xx}), \\ T_2 &= 2\psi_{xy}(\zeta_{xx} - \zeta_{yy}) - 2\zeta_{xy}(\psi_{xx} - \psi_{yy}), \\ T_3 &= 2(\psi_y\zeta_{yyx} + \zeta_x\psi_{xxy} - \psi_x\zeta_{xxy} - \zeta_y\psi_{yyx}). \end{aligned}$$

It is clear that each term in T_1, T_2 and T_3 can be approximated up to $O(h^2)$ within the nine-point stencil. We quote some samples of the difference formulae to be used:

$$u_{xx} = \frac{u_1 + u_3 - 2u_0}{h^2} + O(h^2), \qquad u_{xy} = \frac{u_5 - u_6 + u_7 - u_8}{4h^2} + O(h^2),$$

$$u_x = \frac{u_1 - u_3}{2h} + O(h^2), \qquad u_{xxy} = \frac{u_5 + u_6 - u_7 - u_8 - 2(u_2 - u_4)}{2h^3} + O(h^2).$$

Finally we obtain

$$\begin{aligned} T_1 &= \frac{Re}{4h^4}\left[\psi_{13}\zeta_{13}\psi_{204} + \psi_{24}\zeta_{24}\psi_{103} + \tfrac{1}{2}\psi_{13}\psi_{24}(\zeta_{56} + \zeta_{78}) - \tfrac{1}{4}(\psi_{13}\zeta_{24} + \psi_{24}\zeta_{13})(\psi_{56} + \psi_{78})\right. \\ &\quad \left. -\psi_{13}^2\zeta_{204} - \psi_{24}^2\zeta_{103}\right] + O(h^2), \\ T_2 &= \frac{1}{2h^4}(\psi_{56} + \psi_{78})(\zeta_{12} + \zeta_{34}) - \frac{1}{2h^4}(\zeta_{56} + \zeta_{78})(\psi_{12} + \psi_{34}) + O(h^2), \\ T_3 &= -\frac{2}{h^4}\zeta_{13}\psi_{24} + \frac{2}{h^4}\psi_{13}\zeta_{24} + \frac{1}{2h^4}\psi_{24}(\zeta_{56} - \zeta_{78}) + \frac{1}{2h^4}\zeta_{13}(\psi_{57} + \psi_{68}) - \frac{1}{2h^4}\zeta_{24}(\psi_{56} - \psi_{78}) \\ &\quad - \frac{1}{2h^4}\psi_{13}(\zeta_{57} + \zeta_{68}) + O(h^2). \end{aligned}$$

Substituting the above results into (20) and using (16), we obtain the fourth-order compact scheme (7).

REFERENCES

1. G. Q. Chen, Z. Gao and Z. F. Yang, *J. Comput. Phys.*, **104**, 129 (1993).
2. S. C. R. Dennis and J. D. Hudson, *J. Comput. Phys.*, **85**, 390 (1989).

3. M. M. Gupta, *J. Comput. Phys.*, **93**, 343 (1991).
4. M. M. Gupta, R. Manohar and J. W. Stephenson, *Numer. Methods Partial Diff. Eqns*, **1**, 71 (1985).
5. M. M. Gupta and R. P. Manohar, *J. Comput. Phys.*, **31**, 265 (1979).
6. B. Fornberg, *J. Comput. Phys.*, **61**, 297 (1985).
7. C. W. Richards and C. M. Crane, *Appl. Math. Model.*, **3**, 205 (1979).
8. J. S. Bramley and D. M. Sloan, 'A comparison of an upwind scheme with a central difference scheme for moderate Reynolds number', *Department Report 3*, Department of Mathematics, University of Strathclyde, Glasgow, 1988 (unpublished).
9. U. Ghia, K. N. Ghia and C. T. Shin, *J. Comput. Phys.*, **48**, 387 (1982).
10. R. Schreiber and H. B. Keller, *J. Comput. Phys.*, **49**, 310 (1983).
11. P. M. Gresho, *Ann. Rev. Fluid Mech.*, **23**, 413 (1991).
12. H. Huang and H. Yang, 'The computational boundary method for solving the Navier–Stokes equations', *Research Report*, Institute of Applied Mathematics, University of British Columbia, 1990 (unpublished).
13. T. Y. Hou and B. T. R. Wetton, *SIAM J. Numer. Anal.*, **29**, 615 (1992).
14. H. Nishida and N. Satofuka, *Int. J. Numer. Methods Eng.*, **34**, 637 (1992).
15. B. Fornberg, 'Computing steady incompressible flows past blunt bodies—a historical overview', in M. J. Baines and K. W. Morton (eds), *Numerical Methods for Fluid Dynamics IV*, Oxford University Press, Oxford, 1993, pp. 115–134.
16. F. T. Smith, *J. Fluid Mech.*, **92**, 171 (1979).
17. T. Y. Hou and B. T. R. Wetton, 'Stable fourth order stream-function methods for incompressible flows with boundaries', submitted.
18. A. M. Berger, J. M. Solomon, M. Ciment, S. H. Leventhal and B. C. Weinberg, *Math. Comput.*, **35**, 695 (1980).
19. J. C. Strikwerda, *Finite Difference Schemes and Partial Differential Equations*, Wadsworth & Brooks/Cole, 1989.